**Astronomy & Astrophysics**

# GalaPy: A highly optimised C++/Python spectral modelling tool for galaxies

## I. Library presentation and photometric fitting

T. Ronconi[1,2,3,11], A. Lapi[1,2,4,5], M. Torsello[1], A. Bressan[1], D. Donevski[6,1], L. Pantoni[7], M. Behiri[1], L. Boco[1], A. Cimatti[8], Q. D'Amato[9], L. Danese[1], M. Giulietti[1], F. Perrotta[1], L. Silva[10], M. Talia[8], and M. Massardi[4,1]

1 Scuola Internazionale Superiore di Studi Avanzati (SISSA), Via Bonomea 265, 34136 Trieste, Italy
  e-mail: tronconi@sissa.it
2 Institute for Fundamental Physics of the Universe (IFPU), Via Beirut 2, 34151 Trieste, Italy
3 INAF – Osservatorio di Astrofisica e Scienza dello Spazio (OAS), Via Gobetti 93/3, 40127 Bologna, Italy
4 IRA-INAF, Via Gobetti 101, 40129 Bologna, Italy
5 INFN-Sezione di Trieste, Via Valerio 2, 34127 Trieste, Italy
6 National Centre for Nuclear Research, Pasteura 7, 02-093 Warsaw, Poland
7 Sterrenkundig Observatorium Universiteit Gent, Krijgslaan 281 S9, 9000 Gent, Belgium
8 Dip. Fisica e Astronomia 'Augusto Righi', Univ. Bologna, Viale Berti Pichat 6/2, 40127, Bologna, Italy
9 INAF – Osservatorio Astrofisico di Arcetri, Largo Enrico Fermi, 5, 50125 Firenze, FI, Italy
10 INAF-OATS, Via Tiepolo 11, 34143 Trieste, Italy
11 ICSC – Centro Nazionale di Ricerca in High Performance Computing, Big Data e Quantum Computing, Via Magnanelli 2, Bologna, Italy

**ABSTRACT**

Bolstered by upcoming data from new-generation observational campaigns, we are about to enter a new era in the study of how galaxies form and evolve. The unprecedented quantity of data that will be collected from distances that have only marginally been grasped up to now will require analytical tools designed to target the specific physical peculiarities of the observed sources and handle extremely large datasets. One powerful method to investigate the complex astrophysical processes that govern the properties of galaxies is to model their observed spectral energy distributions (SEDs) at different stages of evolution and times throughout the history of the Universe. To address these challenges, we have developed GalaPy, a new library for modelling and fitting SEDs of galaxies from the X-ray to the radio band, as well as the evolution of their components and dust attenuation and reradiation. On the physical side, GalaPy incorporates both empirical and physically motivated star formation histories (SFHs), state-of-the-art single stellar population synthesis libraries, a two-component dust model for attenuation, an age-dependent energy conservation algorithm to compute dust reradiation, and additional sources of stellar continuum such as synchrotron, nebular and free-free emission, as well as X-ray radiation from low- and high-mass binary stars. On the computational side, GalaPy implements a hybrid approach that combines the high performance of compiled C++ with the user-friendly flexibility of Python. Also, it exploits an object-oriented design via advanced programming techniques. GalaPy is the fastest SED-generation tool of its kind, with a peak performance of almost 1000 SEDs per second. The models are generated on the fly without relying on templates, thus minimising memory consumption. It exploits a fully Bayesian parameter space sampling, which allows for the inference of parameter posteriors and thereby facilitates the study of the correlations between the free parameters and the other physical quantities that can be derived from modelling. The application programming interface (API) and functions of GalaPy are under continuous development, with planned extensions in the near future. In this first work, we introduce the project and showcase the photometric SED fitting tools already available to users. GalaPy is available on the Python Package Index (PyPI) and comes with extensive online documentation and tutorials.

**Key words.** methods: data analysis – galaxies: evolution – galaxies: high-redshift – galaxies: photometry

## 1. Introduction

Galaxies are extremely complex astrophysical objects resulting from the processes affecting baryonic matter after its collapse within dark matter halos. Their formation and evolution strongly depend on the interplay of several factors, including their matter reservoir and accretion history, their environment and possible interactions with neighbours and, ultimately, the large scale structure of the Universe and the physics regulating it on cosmological scales. By studying the properties of individual galaxies, such as their luminosity, stellar mass, chemical composition, and star formation history, we can learn how such objects form and

evolve over time as well as the cosmological conditions that lead to their assembly.

The broadband spectral energy distribution (SED) of a galaxy describes the distribution of its light across the electromagnetic spectrum, from gamma rays to radio waves, and bears the imprints of the baryonic components and processes determining its evolutionary history. Galaxy SEDs constitute primary tools of extra-galactic astronomy to constrain models of galaxy formation and evolution, which are an essential part for our understanding of the Universe as a whole. The majority of commonly used SED fitting tools (e.g. Da Cunha et al. 2008; Chevallard & Charlot 2016; Carnall et al. 2018;

Boquien et al. 2019; Johnson et al. 2021; Vidal-García et al. 2024; Doore et al. 2023) have mainly been developed for studies of low-redshift objects, thus providing the user with empirical fitting recipes that are (mostly) constrained in the local Universe. Even though such tools have been extensively used in constraining the physical properties of galaxies, even at high redshift, they lack a physically motivated interplay between the recipes they use and the actual evolution of the modelled galaxy SED over cosmic time. In several studies, this has required some tweaking and hacking, especially when it comes to the high-redshift Universe (Novak et al. 2017; Jin et al. 2018; Wang et al. 2019; Gruppioni et al. 2020; Pantoni et al. 2021; Talia et al. 2021; Giulietti et al. 2023; Enia et al. 2022; Jin et al. 2022; Castellano et al. 2022; Rodighiero et al. 2022; Finkelstein et al. 2023). Moreover, since the quality and spectral resolution of the SEDs in high-$z$ galaxies are typically much worse than for local objects, a detailed modelling of spectral features can be traded off for a focus on the quantities crucial to derive information about the star formation histories, dust content, and properties of the interstellar medium (see, e.g. Förster Schreiber & Wuyts 2020; Tacconi et al. 2020, for two reviews on high redshift galaxies and the evolution of their content).

On the theoretical side, investigating the SEDs of high-$z$ galaxies can inform us about the evolution of the overall galaxy population across cosmic times. For example, one crucial issue in galaxy evolution concerns the formation of local quiescent galaxies; the issue can (in principle) be resolved by investigating the SEDs of their high-redshift progenitors, which are thought to be dust-enshrouded star-forming objects forming most of their stars at $z \gtrsim 2$, during the so-called cosmic noon or further back in time during cosmic dawn, at $z \gtrsim 3$ (Shapley 2011; Lapi et al. 2018; Gruppioni et al. 2020; Talia et al. 2021). In addition, more physical (but also time-consuming) radiative transfer SED models (e.g. Silva et al. 1998; Camps & Baes 2020) are not suitable for application to the large observational datasets that are available.

In fact, on the observational side, ongoing and upcoming experiments are (and will continue to be) producing an ever-increasing amount of data from galaxies at high redshifts. For example, ALMA has opened a window up to redshift $z \sim 8$ in the (sub-)millimetre bands (see e.g. Walter et al. 2012; Simpson et al. 2014, 2017, 2020; Brisbin et al. 2017; González-López et al. 2017; Scoville et al. 2017; Franco et al. 2018; Bischetti et al. 2019; Dudzevičiūtė et al. 2020; Gruppioni et al. 2020; Pensabene et al. 2020, 2021; Hodge & da Cunha 2020; Smail et al. 2021; Ferrara et al. 2022; Hamed et al. 2023). Meanwhile, JWST is investigating the Universe in the observed near-IR (NIR) bands, both in photometry and spectroscopy, out to the Epoch of Reionization (EoR) and beyond (e.g. Castellano et al. 2022; Naidu et al. 2022; Labbé et al. 2023; Finkelstein et al. 2022; Adams et al. 2023; Atek et al. 2023; Harikane et al. 2023; Yan et al. 2023); these data complement the already available multi-wavelength datasets from large high-$z$ observational campaigns, such as the Great Observatories Origins Survey (GOODS, Giavalisco et al. 2004), *Hubble* Ultra-Deep Field (HUDF, Beckwith et al. 2006), and COSMOS (Scoville et al. 2007), as well as data from deep and large-area blind surveys in the infrared domain, such as PACS Evolutionary Probe (PEP, Lutz et al. 2011), *Herschel* Multi-tired Extra-galactic Survey (Her-MES, Oliver et al. 2012), *Herschel* Astrophysical Terahertz Large Area Survey (H-ATLAS, Eales et al. 2010), and *Herschel* Extragalactic Legacy Project (HELP, Shirley et al. 2019, 2021). Ongoing experiments, such as the Evolutionary Map of the Universe (EMU, Norris et al. 2021),

performed with ASKAP (Johnston et al. 2007, 2008; McConnell et al. 2016; Hotan et al. 2021) and the MeerKAT (Booth & Jonas 2012; Jonas & MeerKAT Team 2016) International GHz Tiered Extragalactic Exploration (MIGHTEE, Jarvis et al. 2016; Taylor & Jarvis 2017), are tackling sensitivities never achieved before at the longest wavelengths of the extra-galactic emission spectrum. These latter experiments are nonetheless only pathfinders for the unprecedented amount of data and scientific information that will be collected by the Square Kilometre Array Observatory (SKAO, Blyth et al. 2015) in the same wavelength range. In a complementary way, the *Euclid* mission (Amendola et al. 2018) with its visible imager (VIS, Cropper et al. 2016) and near infrared imaging photometer (NIP, Schweitzer et al. 2010), along with the *Vera C. Rubin* Observatory and its Legacy Survey of Space and Time (LSST, LSST Science Collaboration 2009), as well as the Dark Energy Spectroscopic Instrument (DESI, DESI Collaboration 2016), will probe the visible and infra-red regions of the spectrum on extremely wide areas and high sensitivities.

In this work, we present GalaPy, an extensible application programming interface (API) for modelling broadband galaxy SEDs with a particular focus on high-redshift objects[1]. It provides an easy-to-use Python user interface while the number-crunching is done with compiled, high-performance, object-oriented C++. The development of this tool is an ongoing project and the software has been designed to envisage modelling extensions and computational upgrades that are already planned and under development.

In the deepest extra-galactic fields, such as COSMOS, the large amount of high-quality, panchromatic data requires not only the derivation of physical parameters, but also their interpretation. One possibility to tackle this point, is to provide informative priors on the model defining parameters, in GalaPy this is guaranteed by the implemented Bayesian framework, which provides an interface to sophisticated statistical analysis, not possible with template-fitting codes. Another possible approach is to directly include physical models (e.g. analytic solutions for galaxy evolution) within the SED modelling and fitting code. This solution seems particularly important in the era of the large programs outlined above (e.g. synergy between JWST, ALMA, *Euclid*, and LSST) that aim to explore the co-evolution of stars, dust, gas, and metals. Indeed, in spite of its potential importance, many previous SED models have not considered the co-evolution of all these components in a physically consistent manner. To this end, along with more classical empirically motivated models, we have implemented a physically motivated model of star formation history (SFH): the in situ model based on works from Lapi et al. (2018, 2020) and Pantoni et al. (2019). With this model, it is possible to get to an analytical estimate of various physical quantities characterising a galaxy, such as its dust and gas content as well as its metallicity. It is mainly designed to interpret the emission of highly star forming galaxies that end up in local early type galaxies, along all their evolution from the highest to the lowest redshifts, and it also proves effective in modelling local late-type galaxies.

As it is being confirmed by JWST since it started taking data, the high redshift Universe is populated by objects that are intensively star-forming and (crucially) highly obscured. Dust plays a main role in shaping the emission of galaxies, especially in the earliest phases of evolution, but it is not granted that its absorption properties at high redshift can be safely

---

[1] GalaPy can be installed from the Python Package Index: `pypi.org/project/galapy-fit`. The documentation is available at: `galapy.readthedocs.io/en/latest/index.html`

modelled with attenuation laws empirically derived from observations of the low redshift Universe. The approach we implement in GalaPy to model dust is inspired by the one presented in the classical GRASIL code (Silva et al. 1998), with two dust components: one for the age-dependent evolution of molecular clouds around star-forming regions and the other for diffuse dust, distributed on larger scales along the galaxy structure. Differently from GRASIL, we account for the twofold role of dust, which obscures the emission at short wavelengths and re-emits at longer wavelengths, with an age-dependent energy conservation algorithm. This approach, while being physically motivated, keeps the execution time extremely contained with respect to radiative transfer algorithms. With our dust model we can derive non-parametric total attenuation laws, blind to assumptions on the grain physics, and with two components that contribute to the emission blend, thereby shaping the dust emission peak.

In this work we showcase the current status of the project and we demonstrate its power for modelling broadband photometric datasets. The structure of the paper is as follows. In Sect. 2, we describe in detail all the physical models currently delivered with GalaPy. In Sect. 3, we discuss the statistical inference tools used for sampling the parameter space. In Sect. 4, we show the results of the thorough validation tests we performed to verify reliability of the results and demonstrate the potential of our tool. Finally, in Sect. 5, we summarise the key results presented in this manuscript. We note that in Appendix C, we provide a primer on installation and usage of the package. Throughout the work, we adopt the standard, flat $\Lambda$CDM cosmology from Planck Collaboration VI (2020) with rounded parameter values: matter density, $\Omega_M \approx 0.3$; baryon density, $\Omega_b \approx 0.05$; Hubble constant $H_0 = 100\,h$ km s$^{-1}$ Mpc$^{-1}$ with $h \approx 0.7$. A Chabrier (Chabrier 2003) initial mass function is assumed.

## 2. Library models

In this section, we introduce the physics modelled by the GalaPy library. All the physical components and processes have been implemented in separate modules, with the requirement of making each component and process self-consistent, meaning that every module (and therefore any physical process) can be imported and used as a stand-alone module of the library.

Conveniently, a master class `galapy.Galaxy.GXY` wraps-up all of the physical modules described in this section, dealing with the interplay between different parameters and components. The latter allows for computing straightforwardly the overall emission and derived quantities for a given set of parameters, enhancing the general user-friendliness of the workflow. This class is meant to help the user accessing directly all the functionalities of the models already implemented in the library with minimal effort, as well as to ease the correct setting of the parameters that are interdependent among the different modular components. It is nonetheless always possible to customise the workflow by accessing the API, importing functions and classes from the different modules into which the GalaPy library is organised[2].

Along the rest of this section we provide a detailed description of all the physics currently implemented in GalaPy. We refer the reader to Appendix B.2 for a complete list of all the

possible free parameters that can be selected when fitting observational data. Table B.3 provides a handy conversion between the symbol uniquely identifying a parameter in the library and the mathematical symbol used in this manuscript, along with a short description and a reference to locate the position in text where the parameter is used.

### 2.1. Star formation history

Implemented in the `galapy.StarFormationHistory` module, the SFH object allows for the selection of various parametric and non-parametric star-formation history models. GalaPy offers the possibility to use standard empirical models of SFH (Sect. 2.1.1) as well as non-parametric models (Sect. 2.1.2). However, the default SFH model, namely, the in situ model by Lapi et al. (2018; Sect. 2.1.3), has proven particularly successful in predicting the evolution of massive proto-elliptical galaxies and it is also very promising in explaining the fast formation of relatively massive galaxies at $z \gtrsim 10$, one of the key regimes probed by modern observational campaigns (e.g. JWST, SKAO). A quick summary of the parameterised SFRs provided by the different models follows:

– Constant SFR:

$$\psi(t) = \psi_0, \tag{1}$$

where $\psi_0$ is a constant floating-point value expressed in units of $M_\odot$ yr$^{-1}$.

– Generalised version of the delayed exponential SFR:

$$\psi(t) \propto \tau^\kappa \exp(-\tau/\tau_\star), \tag{2}$$

where $\tau_\star$ is the characteristic star-formation timescale and $\kappa$ is a shape parameter for the early evolution; $\kappa = 0$ corresponds to a pure exponential, while $\kappa = 1$ to the standard delayed exponential.

– Log-normal SFR:

$$\psi(t) \propto \frac{1}{\tau} \frac{1}{\sqrt{2\pi\sigma_\star^2}} \exp\left[-\frac{\ln^2(\tau/\tau_\star)}{2\sigma_\star^2}\right]; \tag{3}$$

where $\tau_\star$ and $\sigma_\star$ control the peak age and width.

– In situ physically motivated model (Lapi et al. 2018, 2020; Pantoni et al. 2019):

$$\psi(t) \propto e^{-x} - e^{-s\gamma x}, \tag{4}$$

where $x \equiv \tau/s\tau_\star$ with $s \approx 3$ a parameter related to gas condensation, while $\gamma$ is a parameter including gas dilution, recycling and the strength of stellar feedback (see Lapi et al. 2020, for details), whose value is described in Sect. 2.1.3.

We also allow for the existence of an eventual quenching event that stops the star formation. This is modelled with a heaviside function, multiplying the SFR of choice, which is 1 before $\tau_{\text{quench}}$ and 0 afterwards. The above rates are plotted for fixed values of the parameters in Fig. 1 where we also show the effect of assuming an abrupt quenching event happening at an age of $\tau \approx 10^9$ yr. We note that, in this first version of the library, we only consider the primary episode of star formation, not secondary bursts that will be included in future updates of the package. Nevertheless, pure burst SFHs can be rendered either using the interpolated model or by particular combinations of the free-parameters regulating the shape of the models whose rates are reported above.

---

[2] Detailed tutorials on customisation instructions are (and will be made) available in the project on-line documentation: galapy.readthedocs.io/en/latest/index.html
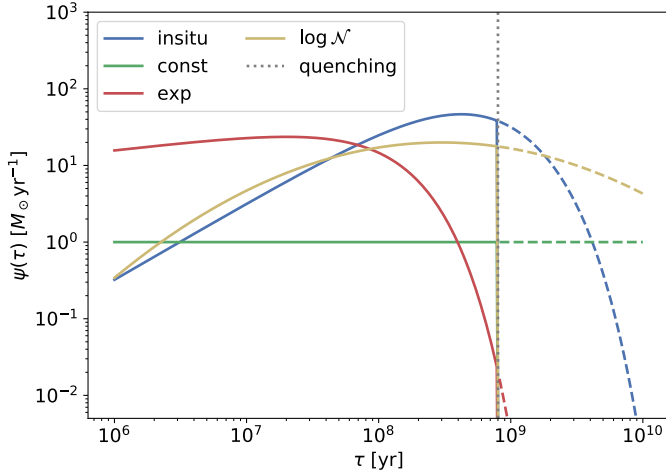
**Fig. 1.** Different models of star formation histories (SFH). Each coloured line shows the star formation rate $\psi$ of a galaxy as a function of its age $\tau$, according to empirical (constant SFR, Eq. (1), green; delayed exponential, Eq. (2) with $\kappa = 1$, red; log-normal, Eq. (3), yellow) and physically-motivated (In situ, Eq. (4): blue line) models. The vertical dotted line marks the age $\tau_{\text{quench}}$ of a possible abrupt quenching event; solid lines refer to the SFH of objects undergoing quenching, while dashed lines to the SFH of objects for which no quenching occurs.

In our chemical evolution model, the stellar mass of a galaxy at a given age, $\tau$, is given by the integral

$$M_\star(\tau) = \int_0^\tau \mathrm{d}\tau' \left[1 - \mathcal{R}(\tau - \tau')\right] \psi(\tau'), \tag{5}$$

where $\mathcal{R}$ is the recycled fraction of gas from stellar evolution. The $\mathcal{R}(\tau)$ factor is given by (see e.g. Cimatti et al. 2020):

$$\mathcal{R}(\tau) = \frac{1}{\psi(\tau)} \int_{m_{\min}(\tau)}^{m_{\max}} \psi(\tau - \tau_{\text{MS}}) \phi(m - m_{\text{rem}}) \mathrm{d}m, \tag{6}$$

where $\tau_{\text{MS}}$ the time spent by a star with mass $m$ in the main sequence, $m_{\text{rem}}$ is the mass of its remnant, $m_{\min}(\tau)$ satisfies $\tau_{\text{MS}}(m_{\min}) = \tau$ and $\phi(m)$ is the Initial Mass Function (IMF). For example, with respect to a Chabrier IMF (Chabrier 2003), it is well approximated by

$$\mathcal{R}(\tau) \approx 0.05 \ln\left(1 + \frac{\tau}{0.4\,\text{Myr}}\right), \tag{7}$$

with typical values around $\mathcal{R} \approx 0.4 \div 0.5$ after $1 \div 10$ Gyr (Pantoni et al. 2019; Lapi et al. 2020); in the instantaneous recycling approximation $\mathcal{R} \approx 0.45$. Even though, at the current state of development, GalaPy implements the aforementioned values only for the case of a Chabrier IMF in the mass range $0.1 \leq M_\star \leq 100$, the library is easily extensible with further models of IMF, including non-standard ones (e.g. Kroupa et al. 2013; Fontanot et al. 2018), that will be added in future releases of the library.

Figure 2 shows the stellar mass growth history corresponding to the models of Fig. 1. As shown in Fig. 2, the overall stellar mass slowly decreases after star formation starts to fade, as a result of the ageing of stellar populations.

### 2.1.1. Empirical models

Most of the SED-fitting libraries available in the literature are delivered with empirical models of SFH (see e.g.
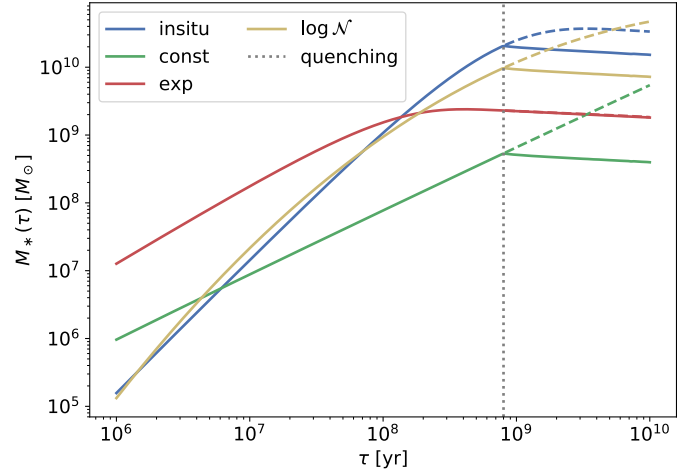


**Fig. 2.** Evolution of the stellar mass $M_\star$ of a galaxy as a function of its age $\tau$, for the SFH models shown in Fig. 1.

Da Cunha et al. 2008; Boquien et al. 2019, for two popular SED-fitting libraries). Such models are primarily motivated by the necessity of reproducing the shape of the cosmic star formation history or, either, to provide a numerically tractable function that returns reasonable values of SFR. A notable exception is Prospector (Johnson et al. 2021), which provides a step-wise tunable SFH module. Even though this approach avoids assumptions on uncertain processes, it ends up in a high dimensional parameter space that slows down inference and reduces accuracy on the parameters estimate.

In tools based on empirical star formation laws, the dust mass, $M_{\text{dust}}$, and the gas (or stellar) metallicity ratio, $Z_{\text{gas}} = Z_\star$, are typically free parameters, while the gas mass is derived on the basis of a (possibly metallicity-dependent) dust-to-gas mass ratio, $D$, gauged on observations. A common expression is (e.g. Tacconi et al. 2018):

$$D_{\text{emp}}(Z) = \frac{M_{\text{dust}}}{M_{\text{gas}}} \approx 0.01 \left(\frac{Z_{\text{gas}}}{Z_\odot}\right)^{-0.85}. \tag{8}$$

In GalaPy, we keep such an approach for backward compatibility and comparison with alternative fitting codes.

### 2.1.2. Interpolated model

We provide a non-parametric, interpolated, step-wise SFH model with derived components (like dust/gas mass and metallicity) treated as free parameters, as in the previous empirical models presented. This model is designed for users willing to predict the emission from galaxies for which the stellar mass growth history is available (e.g. obtained from hydrodynamical simulations or with semi-analytical models) or to test the behaviour of exotic and arbitrarily complex SFH shapes.

In Fig. 3, we show an example of this non parametric model. In the upper panel we plot "observed" samplings of a simulated galaxy's SFH (blue markers with error bars) and the up-sampled prediction of our interpolated model (dashed grey line). On the lower panel we show the stellar mass growth history resulting from integrating the interpolated SFH along the time coordinate.

### 2.1.3. In situ model

The In situ SFH delivered as default in GalaPy implements the (mostly analytic) galaxy formation model first presented in
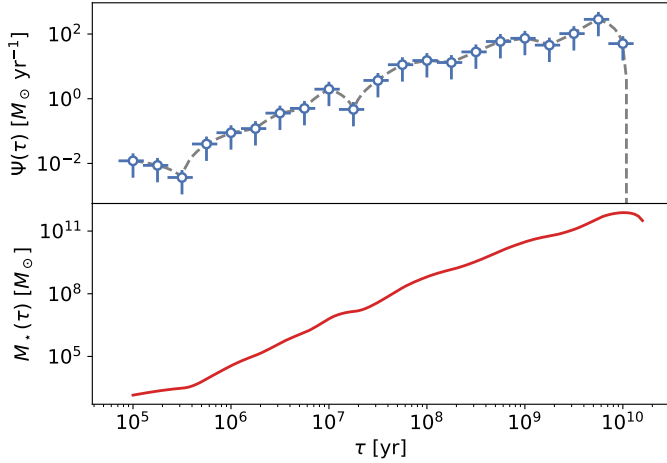
**Fig. 3.** Interpolated SFH model. Upper panel: SFR at different epochs as measured for a simulated galaxy (blue markers with errors) and our interpolated model (dashed grey line). Lower panel: evolution of the integrated stellar mass at different epochs (solid red line) resulting from the SFH interpolated from data in the upper panel.

Lapi et al. (2018) for ETGs, further developed in Pantoni et al. (2019) and extended to LTGs in Lapi et al. (2020). This model is based on a self-consistent treatment of the black-hole/host-galaxy co-evolution, which captures the fast collapse, with low angular momentum, of the innermost gaseous regions of a galaxy and the resulting stellar feedback. Such a regime is extremely important when interpreting the datasets of galaxies at considerable redshift (i.e. $z \gtrsim 4$ and beyond). Furthermore, the model allows for the derivation of age-dependent analytical expressions of the evolution of the gas, metals and dust content in galaxies. Concerning the SFR, the effects of recycling and stellar feedback are encapsulated in the parameter $\gamma$ that appears in Eq. (4) and is defined as:

$$\gamma \equiv 1 - \mathcal{R} + \epsilon_{\text{out}}, \tag{9}$$

in terms of the recycled gas fraction $\mathcal{R}$ of Eq. (7) and of the mass loading factor of the outflows from stellar feedback, $\epsilon_{\text{out}}$. We gauge $\epsilon_{\text{out}} \approx 3[\psi_{\text{max}}/M_\odot \text{yr}^{-1}]^{-0.3}$ according to the hydrodynamic simulations of stellar feedback from Hopkins et al. (2012). Therefore, the parameter $\gamma$ is completely determined in terms of the free parameter $\psi_{\text{max}}$ and, eventually, by the age of the galaxy $\tau$, through Eq. (7).

In the in situ model, the evolution of the gas and dust masses and of the gas and stellar metallicities can be followed analytically as a function of the galactic age and self-consistently with respect to the evolution of the SFR. Specifically, the gas mass is given by

$$M_{\text{gas}}(\tau) = \psi(\tau)\,\tau_\star, \tag{10}$$

while the dust mass,

$$M_{\text{dust}}(\tau) = M_{\text{gas}}(\tau)\,D_{\text{in situ}}(\tau), \tag{11}$$

is computed in terms of the gas mass and of the dust-to-gas mass ratio $D_{\text{in situ}}$. As discussed in Pantoni et al. (2019) and Lapi et al.

(2020), for this latter quantity it is possible to derive an analytical expression, as follows:

$$
\begin{aligned}
D_{\text{in situ}}(\tau) &\approx \frac{s^3\,\epsilon_{\text{acc}}\,y_D\,y_Z}{[s\gamma-1]\,[s(\gamma+\kappa_{\text{SN}})-1]\,[s(\gamma+\tilde{\epsilon})-1]} \\
&\times \left\{1 - \frac{(s\,\gamma-1)\,x}{e^{(s\gamma-1)x}-1}\left[1 + \frac{s\gamma-1}{s\,\tilde{\epsilon}}\left(1 - \frac{1-e^{-s\,\tilde{\epsilon}\,x}}{s\,\tilde{\epsilon}\,x}\right)\right]\right\};
\end{aligned}
\tag{12}
$$

where

$$\tilde{\epsilon} \equiv \kappa_{\text{SN}} + \epsilon_{\text{acc}}\,s\,y_D/[s(\gamma+\kappa_{\text{SN}})-1]. \tag{13}$$

This provides a measure of the efficiency with which dust grains form in terms of the metal coagulation efficiency, $\epsilon_{\text{acc}} \approx 10^6$, onto dust grains, of the dust spallation efficiency $\kappa_{\text{SN}} \approx 10$ by SN shock-waves, and of the dust production yield $y_D \approx 3.8 \times 10^{-4}$.

On the left panel of Fig. 4, we show the evolution of the gas-mass (blue lines) and of the dust-mass (green lines), for the in situ SFH model with the same parameters as for the blue line of Fig. 1. As made evident from the figure, the effect of assuming an abrupt quenching event is to wash out the diffuse matter reservoir of the interested galaxy, that therefore ends up loosing its primary source of star formation and starts ageing.

These authors also derived the following expressions for the gas and stellar metallicity:

$$
\begin{cases}
Z_{\text{gas}}(\tau) \approx \dfrac{s\,y_Z}{(s\gamma-1)}\left[1 - \dfrac{(s\,\gamma-1)\,x}{e^{(s\gamma-1)x}-1}\right], \\[3mm]
Z_\star(\tau) \approx \dfrac{y_Z}{\gamma}\left[1 - \dfrac{s\,\gamma}{s\,\gamma-1}\dfrac{e^{-x}-e^{-s\gamma x}[1+(s\,\gamma-1)\,x]}{s\gamma-1+e^{-s\gamma x}-s\gamma\,e^{-x}}\right],
\end{cases}
\tag{14}
$$

where again $x \equiv \tau/s\tau_\star$, and $y_Z \approx 0.04$ is the metal production yield (already including recycling) for a Chabrier IMF. We show the behaviour of the metallicity evolution of the two different components on the right panel of Fig. 4. As the gaseous component is expected to be enriched more readily with respect to stars, $Z_{\text{gas}}$ is higher than $Z_\star$ consistently along all the evolution history of the galaxy.

Despite being a spatially averaged description of the interplay between the different galaxy components, as well as their evolution, having access to analytical expressions allows us to effectively reduce the volume of the parameter space that has to be sampled for fitting an SED. This not only allows for a faster convergence to an optimal SED, but it also increases the accuracy of our estimates. Furthermore, it is worth highlighting that such a consistent interplay between components, as well as the age-evolution of these derived quantities, are not commonly present in SED-fitting libraries based on energy conservation. In this respect, GalaPy constitutes an innovative and powerful tool for providing non-parametric estimates of the components building up galaxies.

### 2.2. Stellar emission

Under the assumption of an Universal IMF, the stellar birthrate of a galaxy can be split (Bressan et al. 1994, see their Eqs. (1)–(3)) in the product of a mass dependent function (i.e. the IMF) and of a time dependent function (i.e. the SFR). In this scenario, the intrinsic luminosity of stars in a galaxy at a given age is
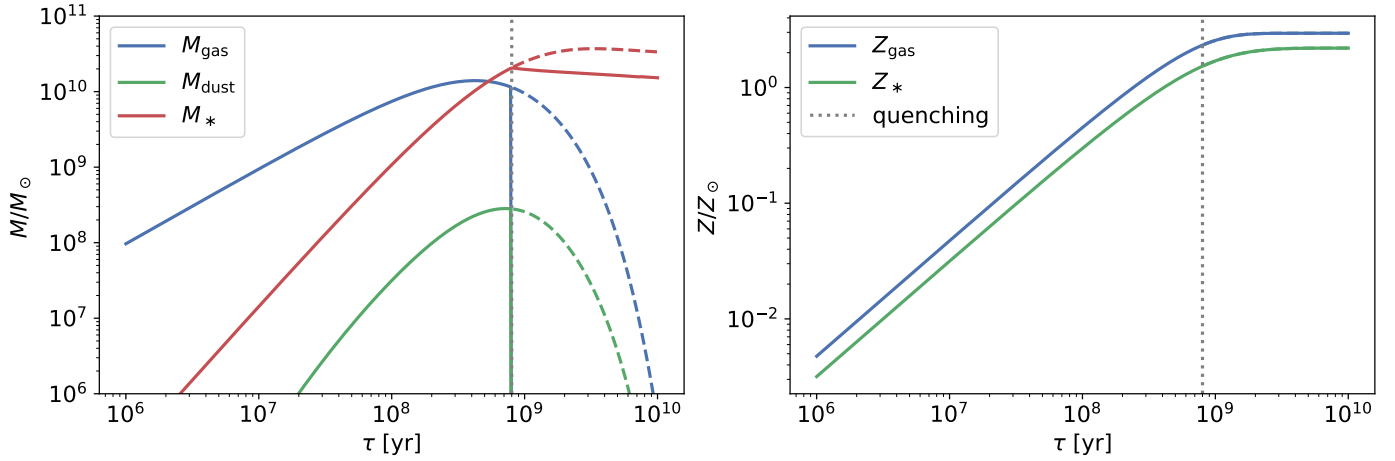
**Fig. 4.** Evolution of various quantities according to the in situ SFH model. Left panel: stellar mass (Eqs. (4)–(5), red), gas mass (Eq. (10), blue) and dust mass (Eq. (11), green). Right panel: gas (blue) and stellar (green) metallicities (Eq. (14)). Linestyles as in Fig. 1.
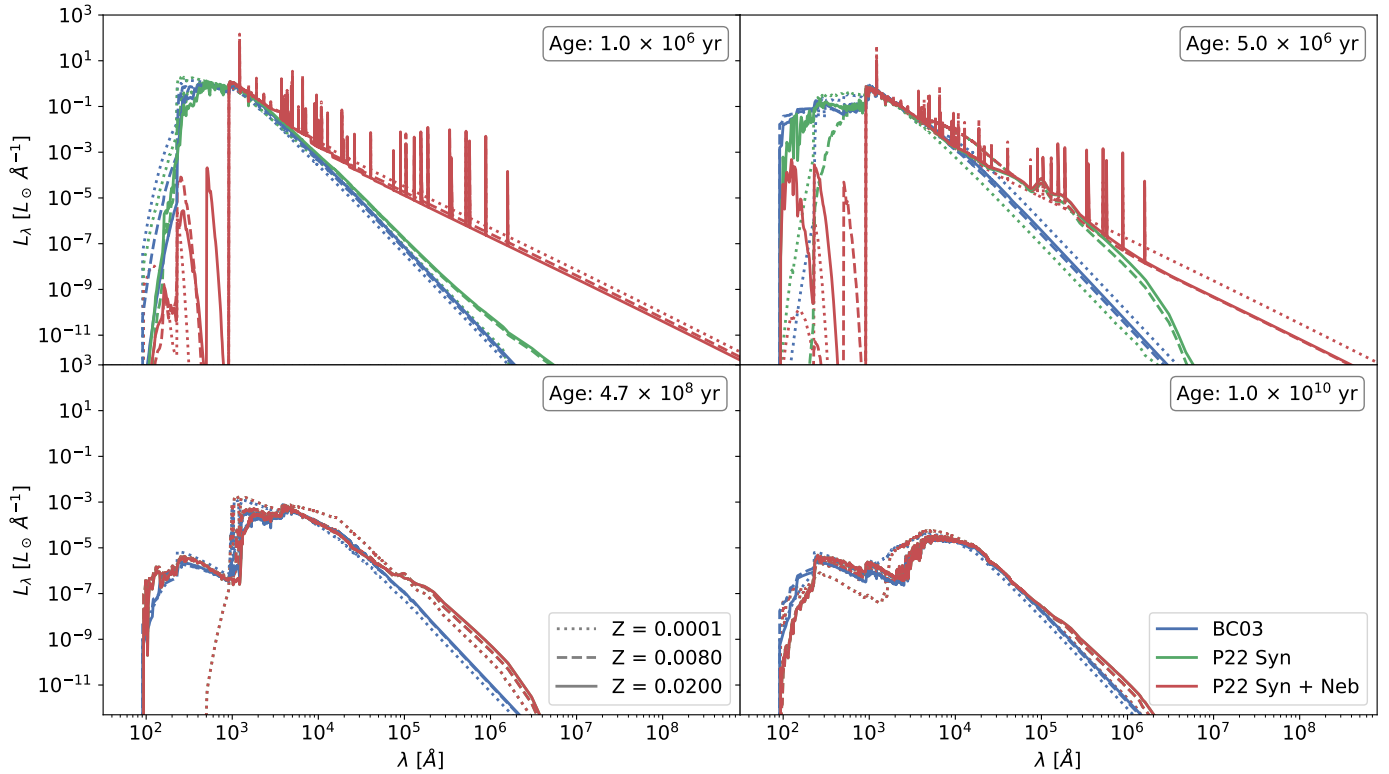


**Fig. 5.** Comparison among the different simple stellar population libraries included in GalaPy: classic BC03 (blue), PARSEC22 without line emission (green), PARSEC22 with line emission (red). Linestyles refer to different metallicity as reported in legend. In all panels the approximate age of the stellar population is reported. In the top two panels we show SSPs from young stellar populations for whom the PARSEC22 models include the contribute of synchrotron (green models) as well as that of nebular emission (red models).

the result of the evolution of the several simple stellar populations (SSPs) that have formed and have aged within the structure in all of its history. Each of the SSPs yields a luminosity $L_{SSP}$ that is computed by the convolution of an initial mass function (IMF), $\phi(m_\star)$, with the luminosity of single stars from stellar evolutionary tracks, $L_{star}$.

$$L_{SSP}(\lambda, \tau, Z) = \int dm_\star \, m_\star \, \phi(m_\star) \, L_{star}(m_\star, \lambda, \tau, Z), \quad (15)$$

where $m_\star$ is the mass of a single star, $\lambda$ is the wavelength, $\tau$ is the age and $Z$ is the metallicity of the given SSP.

In GalaPy we use pre-computed SSP libraries in the form of binary files with specific formatting[3]. In its first release GalaPy is distributed with two main libraries.

– The first one is the classic and popular Bruzual & Charlot (2003) in its updated version (v2016). This library provides the continuum luminosity from SSPs for a set of different IMFs, at varying wavelength, age and metallicity. We refer to these set of libraries as BC03. Blue lines in Fig. 5 show

---

[3] We also provide functionalities to convert eventual custom SSP libraries into the accepted format.

SSPs extracted from this set of libraries, for different metal-licities (different line-styles) and for different ages (different panels).

– As an alternative we have also produced an additional set of SSPs with the PARSEC code (Bressan et al. 2012; Chen et al. 2014, 2015) for a Chabrier IMF and varying ages and metallicities, including emission from dusty AGB stars (Bressan et al. 1998). These libraries come in two flavours, the first one with continuum emission only (green lines in Fig. 5) and the second also including nebular emission (red lines in Fig. 5). In the former, besides continuum stellar emission, non-thermal synchrotron emission from core-collapse supernovae is also included in each SSP spectrum (see, e.g. Vega et al. 2008). In the latter, on top of the stellar continuum and non-thermal synchrotron, nebular emission is also included, with both free-free continuum and nebular emission (see, e.g. Mayya et al. 2004), calculated with CLOUDY (Ferland et al. 1998, 2013, 2017). We refer to these set of libraries as PARSEC22.

We highlight that, using the PARSEC22 SSP libraries come with the advantage of reducing the total amount of computations the code has to perform for getting to a final equivalent SED. Namely, using our custom SSP libraries avoids the need to compute the radio stellar emissions that otherwise would require building the synchrotron and nebular free-free contributions described in Sect. 2.4. Furthermore, nebular line emission is currently only available with the PARSEC22 SSP libraries. We refer the reader to Appendix B.1 for further discussion on the differences between the two SSP libraries distributed with GalaPy.

At a given age $\tau$ a galaxy that has followed a SFH $\psi(\tau)$ will host a composite stellar population (CSP) resulting from all the SSPs formed and evolved up to that moment. The overall unattenuated stellar luminosity of the CSP, $L^{\mathrm{i}}_{\mathrm{CSP}}$ (where the superscript "i" stands for intrinsic), is therefore computed by integrating the contribution of SSPs at different ages and stellar metallicities weighted by the formed stellar mass:

$$L^{\mathrm{i}}_{\mathrm{CSP}}(\lambda, \tau) = \int_0^\tau \mathrm{d}\tau_{\mathrm{SSP}} \, L_{\mathrm{SSP}} \left[ \lambda, \tau_{\mathrm{SSP}}, Z_\star(\tau - \tau_{\mathrm{SSP}}) \right] \psi(\tau - \tau_{\mathrm{SSP}}),$$
(16)

where $\tau_{\mathrm{SSP}}$ is the age of the SSP, $L_{\mathrm{SSP}}$ is the luminosity of the SSP per unit stellar mass defined in Eq. (15) and $Z_\star(\tau - \tau_{\mathrm{SSP}})$ is the metallicity of stars at a given instant in the galactic history of metal enrichment. Equation (16) is computed by summing up the light emitted by all the contributing SSPs (as described in Appendix A.1.1 and Eq. (A.1)), the resolution used to compute $\psi(\tau - \tau_{\mathrm{SSP}})$ is fixed at a value $\mathrm{d}\tau = 10^5$ yr. For both the BC03 tables and the PARSEC22 tables, the time domain is sampled on an irregular grid that reaches a maximum accuracy of $\delta\tau = 10^5$ yr.

In Fig. 6, we show the unattenuated stellar emission computed with GalaPy and by integrating Eq. (16) up to different galactic ages. We use our PARSEC22 SSP libraries with nebular emission and integrate them along an in situ SFH with parameters set as for the blue line in Fig. 1 with quenching. We note that the younger CSPs ($\tau = 10^7$ yr in blue and $\tau = 10^8$ yr in green) also show at the longer wavelengths the radio component resulting from the SN synchrotron and nebular emission. It is also worth mentioning that the UV part of the spectrum in the aforementioned CSPs is somewhat depressed as that fraction of the energy budget is absorbed in nebular regions around massive stars and re-emitted by line-transitions.

As a further open question in galaxy evolution is whether the models of IMF developed from studies on the local Universe are representative of stellar populations in the high redshift Universe, we plan to detach from fixed IMF models. In particular and thanks to its object oriented design, the library is already prepared to work with a parameterised IMF. This would mean to integrate Eq. (15) directly instead of getting it from pre-computed libraries.

### 2.3. The age-dependent, two-component dust model

Despite the dust mass in galaxies is usually a few orders of magnitude less than other components (behaviour that is captured by our In situ SFH model, as it is shown in the left panel of Fig. 4), it plays a fundamental role on the emitted spectrum (Draine & Li 2001, 2007; Draine 2011). Interstellar dust grains contribute to a galaxy's spectrum by playing a dual role: they absorb and scatter the intrinsic stellar radiation from CSPs, especially in the UV/optical range, while re-radiating the absorbed energy, primarily in the infrared part of the spectrum.

In GalaPy, we implement an age-dependent, two-component dust model. It comprises a typically hotter molecular cloud phase (in the literature, also referred to as 'birth clouds') and a colder diffuse medium (in the literature, also dubbed a 'cirrus'). The fraction of dust that resides in molecular clouds, $f_{\mathrm{MC}}$ is a free-parameter of the GalaPy model. This parameter anyways assumes typical values around 0.5 and is likely larger in more violently star-forming systems and towards high redshift.

The modelling of the two dust components and of their attenuation and re-radiation has been inspired from previous works, namely from the radiative transfer code GRASIL (Silva et al. 1998), and from popular SED-fitting libraries such as MAGPHYS (Da Cunha et al. 2008), CIGALE (Boquien et al. 2019) and Prospector (Johnson et al. 2021). Like in the latter libraries, GalaPy bypasses the computational cost of radiative transfer by exploiting an energy conservation scheme; however, GalaPy implements energy conservation in an age-dependent way. This means that the attenuation from dust is age-dependent (like in GRASIL) and this in turn determines, via a self-consistent energy conservation calculated time-step by time-step, age-dependent dust temperatures across the galaxy lifetime. Details of such modelling are provided in the rest of this Section, that we divide into two parts for clarity, separating between the two main effects that result from the presence of a dust component, namely attenuation of UV-optical radiation and re-emission in the IR and (sub)mm bands.

#### 2.3.1. Extinction and attenuation

We assume two different, piece-wise extinction curves for the diffuse dust and molecular cloud components (DD and MC, hereafter). The behaviour of the two extinctions is shown in Fig. 7 normalised to their value computed in the $V$-band ($\lambda_V \approx 5500$ Å), $A_V$. This value is parameterised differently for the two components.

For the DD phase we assume an extinction normalisation scaling as

$$A_V^{\mathrm{DD}} = C_V^{\mathrm{DD}} \frac{1 - f_{\mathrm{MC}}}{0.5} \frac{M_{\mathrm{dust}}}{10^8 \, M_\odot} \left( \frac{R_{\mathrm{DD}}}{1 \, \mathrm{kpc}} \right)^{-2},$$
(17)

here $M_{\mathrm{dust}}$ is the dust mass in the galaxy (that can be age dependent if the in situ SFH model is selected), $R_{\mathrm{DD}}$ is the characteristic radius of the diffuse dust component and $C_V^{\mathrm{DD}}$ is
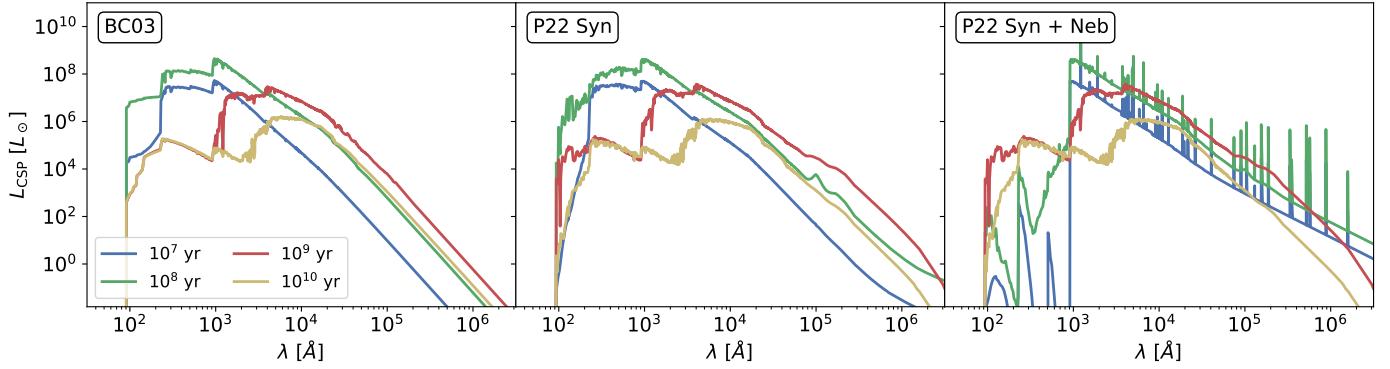
**Fig. 6.** Composite stellar populations as a function of the age, on assuming the in situ SFH (blue line of Fig. 1 with quenching at $\tau = 8 \times 10^8$ yr) and different single stellar population libraries (left: BC03; centre: PARSEC22 without nebular emission; right: PARSEC22 with nebular emission).
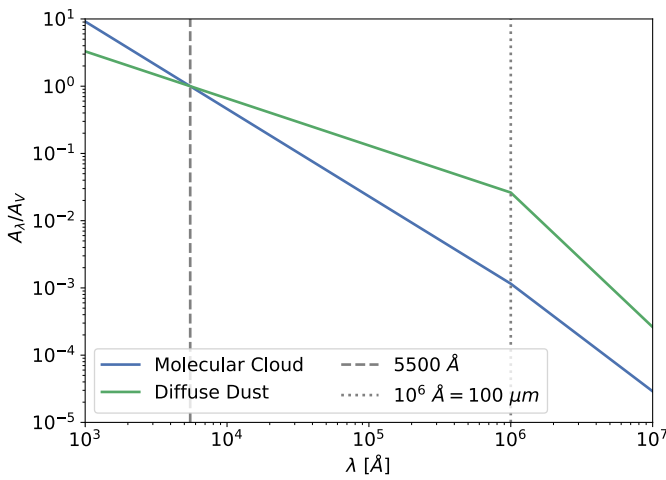


**Fig. 7.** Extinction laws adopted in GalaPy, normalised to the value in the $V-$band at 5500 Å, for diffuse dust (green) and dust in molecular clouds (blue). The extinction is modelled as a double powerlaw (see Eqs. (18)–(20)) with slope changing at around 100 μm (marked with a dotted line; the default values of the slopes are adopted in the plot (see Sect. 2.3 for details).

a normalisation constant of order unity. The extinction law for the diffuse component is prescribed to follow the piece-wise power-law behaviour

$$A_{\rm DD}(\lambda) = A_V^{\rm DD} \left( \frac{\lambda}{5500\,\text{Å}} \right)^{-\delta_{\rm DD}^{\rm l/u}},\qquad(18)$$

with $\delta_{\rm DD}^{\rm l}$ taking on values of around $\approx 0.7$ for $\lambda \lesssim 100\,\mu$m and $\delta_{\rm DD}^{\rm u} \approx 2$ for $\lambda \gtrsim 100\,\mu$m; nonetheless GalaPy allows us to give up on these two reference values by directly fitting the parameters $\delta_{\rm DD}^{\rm l}$ and $\delta_{\rm DD}^{\rm u}$. In Fig. 7, we mark the normalised DD extinction law with reference slopes with a green line.

The piece-wise behaviour imposed by the relation above results from observations of the different cross section of dust grains settling-in at around $\approx 100\,\mu$m. The flatter power-law dependence has been previously assumed by Charlot & Fall (2000) and Da Cunha et al. (2008) basing on the observed relation between the ratio of far-infrared to UV luminosity and the UV spectral slope for nearby starburst galaxies, while the break to a steeper slope reflects the behaviour of the scattering and absorption cross section of dust grains at longer wavelengths (e.g. Silva et al. 1998; Draine & Li 2001).

On the other hand, for the MC component, we adopt a $V$-band extinction

$$A_V^{\rm MC} = C_V^{\rm MC}\, \frac{Z_{\rm gas}}{Z_\odot}\, \frac{f_{\rm MC} M_{\rm gas}}{N_{\rm MC} 10^6\, M_\odot}\, \left( \frac{R_{\rm MC}}{16\,\text{pc}} \right)^{-2},\qquad(19)$$

which is dependent on the average gas mass of a molecular cloud $M_{\rm gas}^{\rm MC}/10^6 M_\odot = (f_{\rm MC} M_{\rm gas})/(N_{\rm MC} 10^6\, M_\odot)$ in units of $10^6\, M_\odot$, on the radius of the cloud $R_{\rm MC}$, on the total number of MCs in the system and on the gas metallicity $Z_{\rm gas}$. The latter dependence is reasonable since within molecular clouds the growth of dust grains is expected to mainly occur via sticking/accretion of metals onto core grains produced during stellar evolution. The normalization $C_V^{\rm MC}$ can be of order several tens to hundreds, since the $V-$band emission in MCs is expected to be completely absorbed. For the MCs we also assume a double power-law extinction curve of

$$A_{\rm MC}(\lambda) = A_V^{\rm MC} \left( \frac{\lambda}{5500\,\text{Å}} \right)^{-\delta_{\rm MC}^{\rm l/u}},\qquad(20)$$

with $\delta_{\rm MC}^{\rm l} \approx 1.3$ for $\lambda \lesssim 100\,\mu$m and $\delta_{\rm MC}^{\rm u} \approx 1.6$ for $\lambda \gtrsim 100\,\mu$m. The former slope corresponds to the middle range of the optical properties of dust grains between the Milky Way, the Large and the Small Magellanic Clouds (see Charlot & Fall 2000; Da Cunha et al. 2008). The slope at long wavelengths, which is slightly shallower than for the diffuse medium, has been advocated to reproduce the sub-mm emission for ULIRGs such as Arp220, where the MC re-radiation dominate over the cirrus' (see Silva et al. 1998; Lacey et al. 2016). MC extinction with reference slopes is shown in Fig. 7 by a blue piece-wise power law. Once again, the slopes can be free-parameters of the model to be fitted directly.

Given the extinction curves of Eqs. (18) and (20), we compute the attenuated galaxy luminosity (i.e. the transmitted one) as

$$L_{\rm CSP}^{\rm a}(\lambda, \tau) = \mathcal{A}_{\rm DD}(\lambda) \times$$

$$\int_0^\tau {\rm d}\tau_{\rm SSP} \mathcal{A}_{\rm MC}(\lambda, \tau_{\rm SSP})\, L_{\rm SSP}[\lambda, \tau_{\rm SSP}, Z_\star(\tau - \tau_{\rm SSP})]\, \psi(\tau - \tau_{\rm SSP}),\qquad(21)$$

where $\mathcal{A}_{\rm DD}(\lambda)$ and $\mathcal{A}_{\rm MC}(\lambda, \tau)$ are the extinction factors due to diffuse and MC dust, respectively, and the superscript 'a' stands for attenuated. We assume the attenuation suffered by radiation
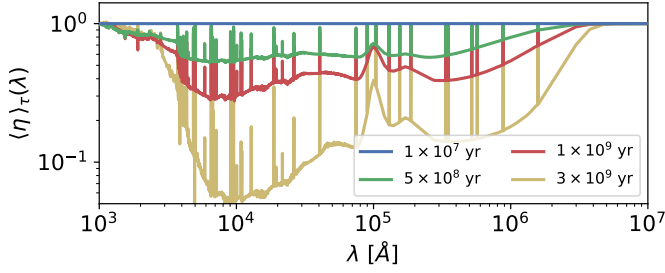
**Fig. 8.** Average fraction of stellar luminosity (see Eq. (27)) that is absorbed by MCs as a function of wavelength for galaxies of different age (colour-coded as in the legend).

from stars that have already escaped their birth MCs to be independent from stellar age; thus the DD extinction factor is simply expressed as:

$$\mathscr{A}_{\mathrm{DD}}(\lambda) = 10^{-0.4\,A_{\mathrm{DD}}(\lambda)}. \tag{22}$$

where $A_{\mathrm{DD}}(\lambda)$ is given by Eq. (18).

On the other hand, since birth clouds tend to be evaporated as the hosted SSPs evolve, the extinction factor due to dust in MCs is defined to be age dependent

$$\mathscr{A}_{\mathrm{MC}}(\lambda) = 1 - \eta(\tau) + \eta(\tau)\,10^{-0.4\,A_{\mathrm{MC}}(\lambda)}, \tag{23}$$

where $\eta(\tau)$ defines the fraction of stars with age $\tau$ still inside their MC. We define this latter quantity taking up from GRASIL the parametrization

$$\eta(\tau) = \begin{cases} 1 & \tau \leq \tau_{\mathrm{esc}} \\ 2 - \dfrac{\tau}{\tau_{\mathrm{esc}}} & \tau_{\mathrm{esc}} < \tau \leq 2\,\tau_{\mathrm{esc}} \\ 0 & \tau > 2\,\tau_{\mathrm{esc}}, \end{cases} \tag{24}$$

with $\tau_{\mathrm{esc}}$ a free-parameter which defines the typical time required by stars to start escaping MCs; after $2\,\tau_{\mathrm{esc}}$ all the stars have escaped.

We can take the luminosity-weighted average over stellar ages of the MC extinction law defined in Eq. (23) and re-write Eq. (21) in compact form:

$$L^{\mathrm{a}}_{\mathrm{CSP}}(\lambda, \tau) = \mathscr{A}_{\mathrm{DD}}(\lambda)\,\langle\mathscr{A}_{\mathrm{MC}}\rangle_\tau(\lambda)\,L^{\mathrm{i}}_{\mathrm{CSP}}(\lambda, \tau), \tag{25}$$

where $L^{\mathrm{i}}_{\mathrm{CSP}}(\lambda, \tau)$ is the intrinsic CSP luminosity of Eq. (16) and

$$\langle\mathscr{A}_{\mathrm{MC}}\rangle_\tau(\lambda) = 1 - \langle\eta\rangle_\tau(\lambda)\left[1 - 10^{-0.4\,A_{\mathrm{MC}}(\lambda)}\right], \tag{26}$$

with

$$\langle\eta\rangle_\tau(\lambda) = \frac{\int_0^\tau \mathrm{d}\tau_{\mathrm{SSP}}\,\eta(\tau_{\mathrm{SSP}})\,L_{\mathrm{SSP}}\left[\lambda, \tau_{\mathrm{SSP}}, Z_\star(\tau - \tau_{\mathrm{SSP}})\right]\psi(\tau - \tau_{\mathrm{SSP}})}{\int_0^\tau \mathrm{d}\tau_{\mathrm{SSP}}\,L_{\mathrm{SSP}}\left[\lambda, \tau_{\mathrm{SSP}}, Z_\star(\tau - \tau_{\mathrm{SSP}})\right]\psi(\tau - \tau_{\mathrm{SSP}})}. \tag{27}$$

We show the behaviour of the latter quantity in Fig. 8 for different galactic ages for a fixed value of $\tau_{\mathrm{esc}} = 5 \times 10^7$ yr. While almost all the radiation is absorbed in the younger objects (blue and green lines) a considerable part of the stellar radiation escapes when the galaxy ages (red and purple lines).
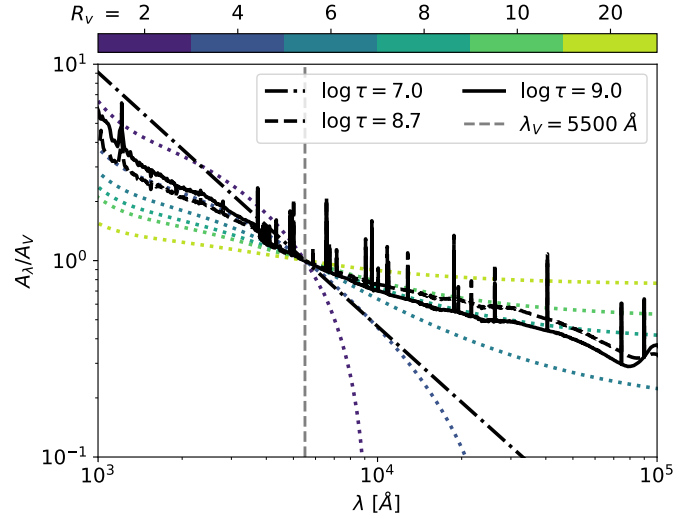


**Fig. 9.** Overall attenuation curve at ages of $10^7$ yr (dot-dashed, i.e. $0.5\tau_{\mathrm{esc}}$), $5 \times 10^8$ yr (dashed, i.e. $10\tau_{\mathrm{esc}}$), and $10^9$ yr (solid, i.e. $20\tau_{\mathrm{esc}}$), we include age effects and plot the value in units of the attenuation in the visible band ($\lambda_V \approx 5500$ Å). We note that these values correspond to the blue, green and red lines of Fig. 8. Our attenuation curves are compared with Calzetti-like attenuation curves (dotted) for different values of the total-to-selective extinction ratio $R_V$ in the $V$−band (colour-coded).

To wrap up, we obtain the wavelength- and age-dependent total galactic attenuation curve, given by

$$A_{\mathrm{TOT}}(\lambda, \tau) = -2.5\log_{10}\left[\mathscr{A}_{\mathrm{DD}}(\lambda)\,\langle\mathscr{A}_{\mathrm{MC}}\rangle_\tau(\lambda)\right], \tag{28}$$

shown in Fig. 9 for galaxies with different age, normalised with respect to the global attenuation in the visible band ($\lambda_V \approx 5500$ Å). The attenuation curves are built assuming the in situ SFH (blue line in Fig. 1) assuming no quenching and a characteristic escape time from MCs of $\tau_{\mathrm{esc}} = 5 \times 10^7$ yr[4]. In young galaxies (dot-dashed black line) all the stellar populations will still be embedded by their birth MC, therefore their global attenuation curve traces the intrinsic extinction of MCs (blue solid line in Fig. 7). Instead, older galaxies (dashed and solid black lines) will host populations of different ages which therefore will provide different contributions to the global attenuation, as some of them will still be embedded in their birth cloud while some others will have partially or completely escaped it. This evolution with time is reflected on the bending of the global attenuation curve and on the peaks due to the presence of intense emission lines, the latter being the imprint of the youngest stellar populations.

It is also interesting to compare our age-dependent attenuation curves with those predicted by Calzetti-like models (Calzetti et al. 2000; Salim & Narayanan 2020). In Fig. 9, curves with different colours mark different values of the total-to-selective extinction ratio in the $V$−band, $R_V$. The shape of Calzetti-like attenuation curves is obtained by empirical considerations on the UV/optical photometry of observed galaxies (Salim & Narayanan 2020). In our dust model we do not rely on templated nor parametric global attenuation curves and we are independent from dust-grain physics models. We, nonetheless,

---

[4] Even though we limit our discussion to the in situ SFH model, all the results can be also obtained using any other SFH model available in the library.
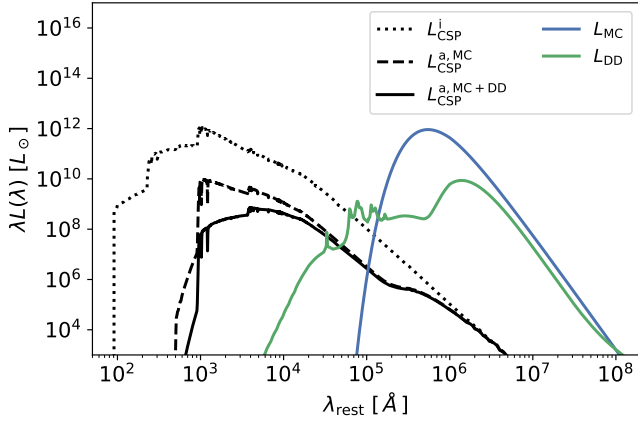
**Fig. 10.** Impact of absorption from the two component dust models (molecular clouds, MC; diffuse dust, DD) implemented in GalaPy on the intrinsic stellar emission (dotted black line). Luminosity escaping from MCs is marked by a dashed black line, while the final stellar emission escaping MCs and DD is shown by a solid black line. The luminosity re-emitted in the IR bands is highlighted with a solid blue line for MCs and with a solid green line for the DD(+PAH) component.

manage to derive shapes similar to those found in the literature by consistently treating the age-evolution and stellar population dependency of the two different dust phases. We derive a model of the global attenuation in a galaxy from data of the transmitted light, by fitting directly the free parameters in from Eqs. (17) to (20) and Eq. (24).

The absorption from the two different components on stellar emission is decomposed in Fig. 10 for a 100 Myr galaxy at the peak of its star formation history and with a characteristic escape time from MCs of $\tau_{esc} = 50$ Myr. While the dotted black line marks the intrinsic stellar emission, $L^{i}_{CSP}(\lambda)$, the dashed black line marks the luminosity escaping from molecular clouds, $L^{a,MC}_{CSP}(\lambda)$, and the solid black line the obscured stellar emission resulting from Eq. (25), $L^{a,MC+DD}_{CSP}(\lambda) = L^{a}_{CSP}(\lambda)$.

We stress that, internally, the overall contribution is computed by integrating numerically Eq. (21), therefore directly obtaining the SSP luminosity averaged value of Eq. (28) (shown in Fig. 9) by computing the ratio between the attenuated and intrinsic luminosity: $L^{a}_{CSP}(\lambda, \tau)/L^{i}_{CSP}(\lambda, \tau)$. The direct time integration of SSPs attenuation is a peculiarity of our library and is intended to provide blindness to the specific attenuation model. This choice has been made so that we do not have to rely on parametric total attenuation models; therefore, we are able to loosen the assumptions on the dust physics. We believe that our model will prove relevant, e.g. in studies of primordial galaxies at the highest redshifts, such as those that are currently being probed by JWST (sources at $z > 4$–6), and, in general, all those cases that lie outside the typical definition range of existing attenuation laws.

Finally, at this stage we do not yet include a treatment of the UV-bump at 2200 Å as observed in the total attenuation of some close-by sources (see e.g. Noll et al. 2009; Salim & Narayanan 2020), nor its possible relation with the PAH emission, as claimed by some authors. We note that the object oriented design of the library allows us to easily extend the dust modelling to include further components, that we may take in considerations for further developments.

### 2.3.2. Energy conservation and emission

By absorbing stellar radiation, dust heats up. The bolometric intrinsic luminosity coming from the CSP hosted by a galaxy

of given age is obtained by integrating Eq. (16) over all the spectrum:

$$L^{i}_{bol}(\tau) = \int_0^\infty d\lambda\, L^{i}_{CSP}(\lambda, \tau). \tag{29}$$

In GalaPy, such luminosity is absorbed in two stages for stars still embedded within their birth cloud: first it has to pass through the MC phase, and then the remainder of this radiation has then to cross the DD region. The amount of bolometric luminosity, $L^{i}_{bol}(\tau)$, which is absorbed by dust in MCs is obtained by filtering the integral above with the age-dependent law defined in Eq. (26):

$$L^{MC}_{abs}(\tau) = \int_0^\infty d\lambda\, [1 - \langle \mathcal{A}_{MC} \rangle_\tau(\lambda)]\, L^{i}_{CSP}(\lambda, \tau). \tag{30}$$

The luminosity that has not been transferred to MCs (i.e. $\left[ L^{i}_{CSP} - L^{MC}_{abs} \right](\lambda, \tau) = \langle \mathcal{A}_{MC} \rangle_\tau(\lambda) L^{i}_{CSP}(\lambda, \tau)$) is then further absorbed by DD:

$$L^{DD}_{abs}(\tau) = \int_0^\infty d\lambda\, [1 - \mathcal{A}_{DD}(\lambda)]\, \langle \mathcal{A}_{MC} \rangle_\tau(\lambda)\, L^{i}_{CSP}(\lambda, \tau). \tag{31}$$

In the left panel of Fig. 11, we show the age-dependency of the percentage of bolometric luminosity that is absorbed by the two different dust phases in units of the typical escape time from MCs, $\tau_{esc}$ defined in Eq. (24). When the stars begin to radiate energy but the galaxy is still younger than the characteristic escape time $\tau_{esc}$, the amount of luminosity absorbed by MCs grows steadily (blue line), while the radiation absorbed by DD is negligible (green line). At an escape time, the percent of luminosity going to MCs instead starts to decrease, while the relevance of the DD component grows. All in all though, the combined effect of the two phases is to trap more than 90% of the total energy budget. This value decreases only at several tens of escape times, when the SFR decreases (see the in situ SFH model marked by a blue line in Fig. 1 and compare to Fig. 9, commented in Sect. 2.3.1) or, either, after an abrupt quenching event that wipes out most of the ISM.

It has to be noted that, in the earliest stages of evolution (i.e. $\tau \approx 10^{-2}\tau_{esc}$) the overall total absorbed fraction of Fig. 11 is of about 0%. This results from the way we compute the evolution of the absorption curves. Namely, in our model this process is strictly dependent on the total budget of absorbing medium that is consistently computed from the evolutionary stage of the stars populating a galaxy. As a consequence, when the galaxy is extremely young (i.e. $\tau \lesssim 10^6$ yr $\equiv 0.1\tau_{esc}$), stars do not have had time yet to pollute the medium with dust and therefore, no absorption is possible.

Energy conservation ensures that (having heated up as a consequence of the luminosity absorbed) the two dust components radiate, in good approximation, as two optically thick grey-bodies. This emission depends on the extinction laws as defined in Eqs. (22) and (23) for the two respective dust phases. We define:

$$L_{DD}(\lambda, \tau | T_{DD}) = \frac{16\pi^2}{3} R^2_{DD}\, [1 - 10^{-0.4 A_{DD}(\lambda, \tau)}]\, B(\lambda, T_{DD}), \tag{32}$$

for the DD phase and

$$L_{MC}(\lambda, \tau | T_{MC}) = \frac{16\pi^2}{3} N_{MC} R^2_{MC}\, [1 - 10^{-0.4 A_{MC}(\lambda, \tau)}]\, B(\lambda, T_{MC}), \tag{33}$$
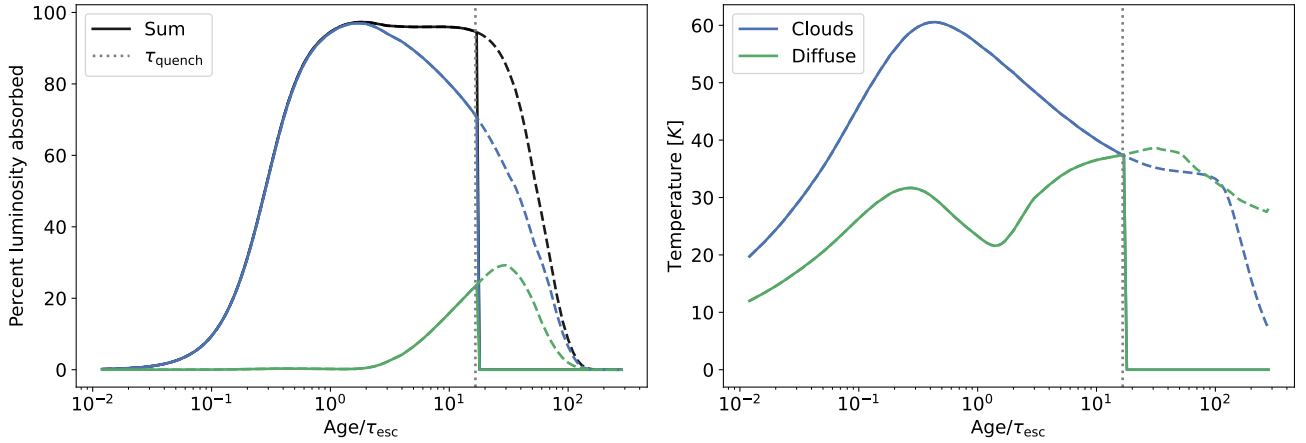
**Fig. 11.** Behaviour of the two different dust components (molecular clouds, MC; diffuse dust, DD) as a function of galactic age in units of the characteristic escape time from molecular clouds $\tau_{esc}$. We assume an in situ SFH as the blue line in Fig. 1 and set the characteristic escape time to $5 \times 10^7$ yr. Left panel: percentage of the intrinsic stellar luminosity absorbed by MC (blue), DD (green), and by both components (black). Right panel: temperature of the dust component computed from the age-dependent energy-conservation scheme implemented in GalaPy. The vertical dotted line marks the age, $\tau_{quench} = 8.8 \times 10^8$ yr, of a possible abrupt quenching event; solid lines refer to the evolution with quenching, dashed lines to that with no quenching.

for the MC phase. Notice that, in the limit of an optically-thin emission, the factor $1-10^{-0.4\,A_{phase}(\lambda)} \approx \rho_{phase}\, k_\lambda\, R_{phase}^3$ is approximately the optical depth, thus, it can be written in terms of the dust-phase density $\rho_{phase}$ and of the opacity $k_\lambda$. Using $\rho_{phase} \approx 3\, M_{phase}/4\,\pi\, R_{phase}^2$, the emitted luminosity can then be recast in the form $L_\lambda \approx 4\,\pi\, M_{phase}\, k_\lambda\, B(\lambda, T_{phase})$, which frequently occurs in the literature (e.g. Lacey et al. 2016).

In both Eqs. (32) and (33), luminosity is given in terms of the black body spectrum:

$$B(\lambda, T) \equiv \frac{2\,h_P c^2}{\lambda^5}\, \frac{1}{e^{h_P\,\nu_\lambda/k_B\,T} - 1} \tag{34}$$

where $\nu_\lambda = c/\lambda$ is the frequency corresponding to the wavelength $\lambda$, $c$ is the speed of light, $h_P$ is the Planck constant and $k_B$ is the Boltzmann constant.

At any given age, the temperatures $T_{DD}$ and $T_{MC}$ of the diffuse and MC dust component are set by requiring that the total emitted power equals the luminosity absorbed by each of the two phases. Therefore, in GalaPy, the dust temperatures are not free parameters, they are age-dependent outputs obtained by imposing a self-consistent energy conservation.

For the emission coming from MCs we impose:

$$\int_0^\infty d\lambda\, L_{MC}[\lambda, \tau\,|\,T_{MC}(\tau)] = L_{abs}^{MC}(\tau), \tag{35}$$

where the left hand side is obtained by integrating over the whole spectrum Eq. (33) and the right hand side has been computed with Eq. (30).

We make the assumption that the emission from polycyclic aromatic hydrocarbons (PAH) is suppressed in MCs, but we include it in the emission coming from the DD phase (Vega et al. 2008). We define a free parameter $0 \leq f_{PAH} \leq 1$ regulating the fraction of absorbed power $L_{abs}^{DD}(\tau)$ that at some given time is re-radiated by PAH. Therefore, the temperature of the DD grey-body is computed by imposing

$$\int_0^\infty d\lambda\, L_{DD}[\lambda, \tau\,|\,T_{DD}(\tau)] = (1 - f_{PAH})\, L_{abs}^{DD}(\tau), \tag{36}$$

where the left hand side is obtained by integrating over the whole spectrum Eq. (32) and the right hand side has been computed

with Eq. (31) excluding the fraction of energy that is radiated by PAH.

By solving numerically the two energy conservation equations, Eqs. (35) and (36), we obtain the temperatures of the two media consistently with their evolution with time. In the right panel of Fig. 11 we show the age evolution of the dust phases' temperature obtained above in units of the characteristic escape time from MCs. Young galaxies display a steady increase in temperature, steeper and some factors larger for the MC component. When the escape time is reached, the temperatures of both MCs and DD begin to decrease. However, while MCs continue to decrease over time, the temperature of DD initially decreases but then begins to increase again. This instant in the evolution of the galaxy is due to the presence of a large number of stars that have escaped their MC and whose energy therefore contributes only to the heating of the DD phase. Depending on the value of the model parameters, the DD medium could also become hotter than MCs, when most of them have been evaporated. It is interesting to notice how in the early stages of evolution, the DD temperature reaches some tens of degrees even though its contribution to absorption in this stage is negligible (cf. left panel of Fig. 11).

We adopt the PAH template $L_{PAH}(\lambda)$ by Da Cunha et al. (2008) constructed on the behaviour in the photo-dissociation regions of the Milky Way. It includes PAH line emission mainly in mid-IR (MIR), PAH continuum emission in the NIR, and NIR continuum emission due to very small, hot dust grains. All in all, the global emission due to diffuse dust including PAH is given by:

$$L_{DD+PAH}(\lambda, \tau) = L_{DD}[\lambda, \tau\,|\,T_{DD}(\tau)] + f_{PAH}\, L_{abs}^{DD}(\tau)\, L_{PAH}^{norm}(\lambda), \tag{37}$$

where $L_{PAH}^{norm}(\lambda) = L_{PAH}(\lambda) / \int_0^\infty d\lambda\, L_{PAH}(\lambda)$ is the normalised PAH spectrum.

The total dust bolometric luminosity is given by the all-spectrum integral

$$L_{dust}(\tau) = \int_0^\infty d\lambda\, [L_{MC}(\lambda, \tau) + L_{DD+PAH}(\lambda, \tau)] = \int_0^\infty d\lambda\, L_{dust}(\lambda, \tau). \tag{38}$$

We note that other definitions exploited in the literature involve this integral over the wavelength range 8–1000 μm (dubbed FIR for far infrared luminosity) or 3–1100 μm (dubbed TIR for total infrared luminosity).

The emission from the two different dust components, including PAH, is shown in Fig. 10. The blue solid line marks the grey-body emission from molecular clouds, as computed from Eq. (33), while the green solid line shows the overall diffuse dust emission, Eq. (37), from both the grey-body of Eq. (32) and PAH.

### 2.4. Additional sources of stellar continuum

The two different SSP libraries delivered with GalaPy provide different recipes for the stellar emission. As already explained in Sect. 2.2, while PARSEC22 libraries have been computed either with supernova synchrotron included and with supernova synchrotron and nebular emission included, the BC03 libraries do not include either of these contributes. To homogenise (and extend to higher energies) the spectral emission due to the stellar component among the different possible SSP library choice, we provide additional (optional) modules for modelling radiative processes that impact mostly on the rest-frame X-ray and radio bands. Thanks to these, we are able to extend the spectral coverage of the library to the overall range $1\,\text{Å} \leq \lambda \leq 10^{10}\,\text{Å}$, independently of the SSP library of choice.

Including these components is optional, as the photometric system of the dataset under study might not cover such an extended range of wavelengths. To have nebular free-free emission (Sect. 2.4.1) and stellar synchrotron (Sect. 2.4.2) when building models with the helper class `galapy.Galaxy.GXY`, the user has to require for radio-support (as these components mostly impact on the radio bands). We note that both nebular free-free and SN-synchrotron might be already present in the SSPs if, as discussed in Sect. 2.2, one of the PARSEC22 libraries is chosen. In this case requiring for radio-support would be redundant and the system will ignore it[5]. Vice-versa, X-ray binaries (Sect. 2.4.3) are considered by requiring for X-ray support, which will also include high energy emission from an eventual AGN as in Sect. 2.5, if required. We underline that, the choice of SSP library should be driven by the dataset studied. In particular, when working with young objects, the attenuation due to line absorption and re-emission has a non-negligible effect also on photometric observations. In such cases is therefore preferable to work with the PARSEC22 library including line-emission.

Figure 12 shows the impact of the additional stellar continuum processes, with respect to the continuum coming from stellar atmospheres and dust. In the rest of this section, we describe how these components are modelled in GalaPy.

### 2.4.1. Nebular free-free

The nebular free-free (NFF) emission is originated in HII regions associated with short-lived ionising massive stars (stars with age $\lesssim 10^7$ yr in simple stellar evolution models). For the intrinsic NFF

---

[5] Specifically, when using PARSEC22 without nebular emission and radio-support is required, the system will automatically include the nebular free-free emission from Sect. 2.4.1 while, when using PARSEC22 with nebular emission and radio support is required, any source of stellar radio continuum is already present in the SSP and therefore the system will ignore the directive. Further details are given in Appendix B.1.
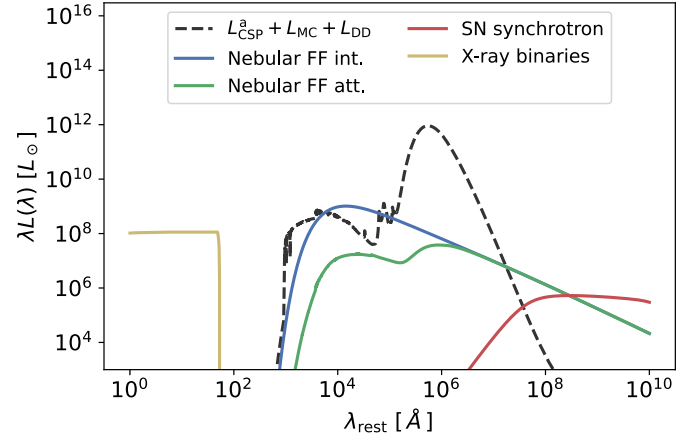
**Fig. 12.** Additional stellar components contributing to the overall continuum emission in GalaPy: intrinsic (blue) and attenuated (green) free-free emission from nebular regions, synchrotron emission from SN (red), X-ray emission from high-mass and low-mass binary stars (yellow). For reference, the luminosity from attenuated stellar continuum and dust re-radiation, i.e. the sum of the solid lines in Fig. 11, is also reported (dashed black).

luminosity (blue solid line in Fig. 12), we use the expression (see, e.g. Bressan et al. 2002; Murphy et al. 2012; Mancuso et al. 2017)

$$L_{\text{NFF}}(\lambda, \tau) \approx 1.8 \times 10^{-27}\,\text{erg s}^{-1}\text{Hz}^{-1}.$$
$$\frac{Q_{\text{H}}(\tau)}{\text{s}^{-1}} \left(\frac{T_e}{10^4\,\text{K}}\right)^{0.3} g_{\text{NFF}}\, \exp\left(\frac{-h_{\text{P}}\,\nu_\lambda}{k_{\text{B}}\,T_e}\right) \quad (39)$$

in terms of the Gaunt factor (see Draine 2011)

$$g_{\text{NFF}} = \ln\left\{\exp\left[5.96 - \frac{\sqrt{3}}{\pi}\ln\left(Z_i\,\frac{\nu_\lambda}{\text{GHz}}\left(\frac{T_e}{10^4\,\text{K}}\right)^{-1.5}\right)\right] + \exp(1)\right\} \quad (40)$$

and of the Boltzmann correction $\exp(-h_{\text{P}}\,\nu_\lambda/k_{\text{B}}\,T_e)$ due to the thermal nature of the process. The latter induces a suppression in the high energy part of the spectrum, due to the decreasing number of high energy photons. In the frequency range satisfying $0.14 < Z_i \nu_9/T_4^{3/2} < 250$ and $\nu_p < \nu < kT/h$, where $\nu_p$ is the plasma frequency, the free-free emission spectrum is almost flat. Such frequencies correspond to the microwave and radio part of the NFF spectrum where it can be shown that the emission slowly declines with increasing frequency as $\sim \nu^{-0.12}$ (Vega et al. 2008; Draine 2011; Mancuso et al. 2017).

In Eq. (40), it is often assumed $Z_i = 1$, corresponding to a pure hydrogen plasma. $T_e$ refers to the electron temperature in HII regions, whose dependence on gas metallicity, $Z_{\text{gas}}$, can be expressed as (Vega et al. 2008)

$$\log T_e \approx 3.89 - 0.4802 \log(Z_{\text{gas}}/0.02) - 0.0205\,[\log(Z_{\text{gas}}/0.02)]^2. \quad (41)$$

The intrinsic photo-ionisation rate can be computed from the intrinsic stellar luminosity of Eq. (16) by the integral

$$Q_{\text{H}}(\tau) = \int_0^{\lambda_{\text{ion}}} \mathrm{d}\lambda\, \frac{L_{\text{CSP}}^{\text{i}}(\lambda, \tau)}{h_{\text{P}}\,\nu_\lambda}, \quad (42)$$

with $\lambda_{\rm ion} \approx 912$ Å being the wavelength corresponding to the H ionisation potential.

In Fig. 12, we also show the attenuation induced by dust in the optical-IR part of the NFF spectrum (solid green line), which is computed as

$$L_{\rm NFF}^a(\tau) = \mathcal{A}_{\rm DD}(\lambda) \langle \mathcal{A}_{\rm MC} \rangle_\tau(\lambda) L_{\rm NFF}^i(\lambda, \tau). \tag{43}$$

where $\mathcal{A}_{\rm DD}(\lambda)$ and $\langle \mathcal{A}_{\rm MC} \rangle_\tau(\lambda)$ are given by Eqs. (22) and (23), respectively. When the SSP chosen is not one among the PARSEC22 libraries with nebular emission included (see Sect. 2.2 and Appendix B.1), this additional source of stellar emission is added a-posteriori to the overall spectrum and, therefore, it is not taken into account automatically in the energy balance described in Sect. 2.3.2. Given that the amount of energy transferred to dust by this process is negligible (i.e. less than 1% in most of the cases), this choice has not a relevant impact for the majority of sources. Nevertheless, for particularly young ages, when the contribution from short lived massive stars is dominant and the energy transferred to nebular emission both in terms of continuum and line emission has a relevant impact also in terms of photometric observations, we recommend using the PARSEC22 SSP libraries with nebular emission included (i.e. `parsec22.ntl` family). This not only guarantees to account for the presence of emission lines but also guarantees that the nebular emission is accounted for in the energy balance algorithm.

### 2.4.2. Synchrotron from supernovae

The synchrotron (non-thermal) emission is likely originated from relativistic electrons accelerated into the shocked interstellar medium, following core-collapse SN explosions. A possible minor contribution from SN remnants is also possible.

When not running with the PARSEC22 SSP libraries, we use the equivalent expression (Bressan et al. 2002; Mancuso et al. 2017)

$$L_{\rm syn}(\lambda, \tau) \approx 10^{30} \, {\rm erg \, s^{-1} Hz^{-1}} \, \frac{\mathcal{R}_{\rm CCSN}(\tau)}{\rm yr^{-1}} \left( \frac{\nu_\lambda}{\rm GHz} \right)^{-\alpha_{\rm syn}}$$
$$\cdot \left[ 1 + \left( \frac{\nu}{20 \, {\rm GHz}} \right)^{0.5} \right]^{-1} F[\tau_{\rm syn}(\nu_\lambda)], \tag{44}$$

where $\mathcal{R}_{\rm CCSN}$ is the core-collapse SN rate, $\alpha_{\rm syn} \approx 0.75$ is the spectral index, the term in square brackets takes into account spectral-ageing effects, and the function $F(x) = (1 - e^{-x})/x$ incorporates synchrotron self-absorption in terms of the optical depth $\tau_{\rm sync} \approx (\nu_\lambda/\nu_{\rm self})^{-\alpha_{\rm syn}-5/2}$ that is thought to become relevant at frequencies $\nu \lesssim \nu_{\rm self} \approx 200$ MHz.

The age-evolution of the CCSN rate per unit solar mass of formed stars has been computed from the SSPs and can be rendered in terms of the simple relation:

$$R_{\rm CCSN}(\tau, Z_\star) \simeq R_0(Z_\star) \, (\tau/{\rm Myr})^{-R_1(Z_\star)}, \tag{45}$$

where $R_0$ and $R_1$ are fitting functions dependent on stellar metallicity (some values are tabulated in Table B.2).

The overall rate entering the expression of the synchrotron luminosity is then

$$\mathcal{R}_{\rm CCSN}(\tau) = \int_0^\tau {\rm d}\tau_{\rm SSP} R[\tau - \tau_{\rm SSP}, Z_\star(\tau - \tau_{\rm SSP})] \psi(\tau - \tau_{\rm SSP}), \tag{46}$$

where, as in Sect. 2.2, $\tau_{\rm SSP}$ is the time passed since some given SSP has formed, $Z_\star(\tau)$ is the metallicity of stars at given galactic age and $\psi(\tau)$ the SFR.

Equation (44) with its normalisation is obtained by requiring that the quantity

$$q_{\rm FIR} \equiv \log \left( \frac{L_{\rm dust}}{3.75 \times 10^{12} \, {\rm W}} \right) - \log \left( \frac{L_{\nu_\lambda = 1.4 \, {\rm GHz}}}{\rm WHz^{-1}} \right) \tag{47}$$

takes on values close to the observed $q_{\rm FIR} \approx 2.35$–$2.7$ at an age of about $10^8$ yr.

To take into account the lower efficiency in producing synchrotron radiation at small SFRs, we correct the above equation as

$$L_{\rm syn}^{\rm corr}(\lambda, \tau) = \frac{L_{\rm syn}(\lambda, \tau)}{1 + [L_{\rm syn}^0/L_{\rm syn}(\lambda, \tau)]^\zeta}, \tag{48}$$

with $\zeta \approx 2$ and $L_{\rm syn}^0 \approx 3 \times 10^{28} \, {\rm erg \, s^{-1} \, Hz^{-1}}$. The corrected synchrotron emission $L_{\rm syn}^{\rm corr}(\lambda, \tau)$ is marked by a red solid line in Fig. 12. We stress that attenuation on the synchrotron emission has been applied but turns out to be irrelevant since the corresponding spectrum is strongly suppressed by self-absorption for wavelengths $\lambda \lesssim 1$ mm.

### 2.4.3. X-ray binaries

The X-ray emission associated with star formation comes mainly from high and low mass X-ray binaries. For their total output, we use the prescriptions by Fragos et al. (2013) based on stellar population synthesis simulation for a Chabrier IMF. Specifically, the contribution to the emission in the 2–10 keV band from high-mass X-ray binaries can be described via the polynomial expression

$$\log(L_{\rm HMXB}/{\rm erg \, s^{-1}}) \approx \log(\dot{M}_\star/M_\odot \, {\rm yr^{-1}}) + 40.28 - 62.12 \, Z_\star$$
$$+569.44 \, Z_\star^2 - 1883.80 \, Z_\star^3 + 1968.33 \, Z_\star^4, \tag{49}$$

while that from low-mass X-ray binaries reads

$$\log(L_{\rm LMXB}/{\rm erg \, s^{-1}}) \approx$$
$$\log(M_\star/M_\odot) + 40.276 - 1.503 \, \theta - 0.423 \, \theta^2 + 0.425 \, \theta^3 + 0.136 \, \theta^4, \tag{50}$$

where $\theta \equiv \log(\tau/{\rm Gyr})$.

We distribute both emissions according to a power-law with an exponential cutoff

$$L_\Gamma^X(\lambda) \propto E^{-\Gamma+3}(\lambda) \, e^{-E(\lambda)/E_{\rm cut}}, \tag{51}$$

with $E(\lambda) = h_{\rm P} \nu_\lambda = h_{\rm P} c/\lambda$ the energy of a photon with wavelength $\lambda$. The photon index is set to $\Gamma \approx 1.6$ for LMXB and to $\Gamma \approx 2.0$ for HMXB (see Fabbiano 2006); the high-energy cutoff is fixed at $E_{\rm cut} \approx 100$ keV, while at the other end the spectrum is extended up to $\lambda \approx 50$ Å.

The resulting total emission from X-ray binaries,

$$L_{\rm XRB}(\lambda, Z_\star, \tau) = L_{\rm HMXB}(Z_\star)L_{\Gamma=2}^X(\lambda) + L_{\rm LMXB}(\tau)L_{\Gamma=1.6}^X(\lambda), \tag{52}$$

is marked by a solid yellow line in Fig. 12.

## 2.5. Active galactic nucleus

The panchromatic emission from galaxies modelled by GalaPy can be enriched by the inclusion of templated spectral models of the emission due to a luminous nuclear component. Even though GalaPy is currently intended for the study of galaxies which are not dominated by an active galactic nucleus (i.e. not AGN-dominated), accounting for this component can be important when trying to refine the inference of the hosting galaxy properties from its overall emission, provided that the AGN properties are known.

We adopted the AGN templates $L_{\mathrm{AGN}}^{\mathrm{temp}}(\lambda)$ by Fritz et al. (2006, F06 hereafter), which have been computed via a radiative transfer model and take into account three components: the accretion disk around the central supermassive black hole, the scattered emission by a surrounding dusty torus, and the thermal dust emission associated with the heated dust.

The overall shape of the template depends on six discrete tunable parameters: the ratio $R_{\mathrm{torus}}^{\mathrm{AGN}}$ of the maximum to minimum radii of the dusty torus, the optical depth $\tau_{9.7}^{\mathrm{AGN}}$ at 9.7 μm, the dust density distribution $r^{\beta} e^{-\gamma |\cos\theta|}$ in terms of two parameters, $\beta$ and $\gamma$, the covering angle, $\Theta$, of the torus, and the viewing angle $\Psi_{\mathrm{los}}^{\mathrm{AGN}}$ between the AGN axis and the line of sight. The template library we are using, by the variation of these six parameters, counts 24 000 spectra among which the user can choose. We further vary the overall contribution of the AGN spectrum over the total galactic emission by an additional parameter, $f_{\mathrm{AGN}}$, defined as the contribution of the AGN to the IR emission from interstellar dust.

Specifically, the fraction $f_{\mathrm{AGN}}$ regulates the fractional intensity of the normalised AGN SED at any given galactic age:

$$L_{\mathrm{AGN}}(\lambda, \tau) = \frac{f_{\mathrm{AGN}}}{1 - f_{\mathrm{AGN}}} \frac{L_{\mathrm{AGN}}^{\mathrm{temp}}(\lambda)}{\int_0^\infty \mathrm{d}\lambda\, L_{\mathrm{AGN}}^{\mathrm{temp}}(\lambda)} L_{\mathrm{dust}}(\tau), \tag{53}$$

where $L_{\mathrm{dust}}(\tau)$ is the bolometric dust luminosity at given galactic age as defined in Eq. (38). This modelling choice is valid for objects where the AGN emission in the IR band is sub-dominant with respect to the inter-stellar dust emission. For this reason and to guarantee that Eq. (53) is not diverging, GalaPy forces $f_{\mathrm{AGN}} < 1$.

We also model the intrinsic X-ray emission coming from the inner parts of the accretion disk. This contribution is added on top of the optical/MIR template and is modelled by adopting the same shape of Eq. (51), with photon index $\Gamma \approx 1.8$ and high-energy cutoff $E_{\mathrm{cut}} \approx 300$ keV. The normalisation in the 2–10 keV band is based on the hard X-ray bolometric correction by Duras et al. (2020):

$$\frac{L_{\mathrm{AGN}}^{\mathrm{bol}}}{L_{\mathrm{AGN}}^{X}} \approx 10.96 \left[1 + \frac{\log(L_{\mathrm{AGN}}^{\mathrm{bol}}/L_\odot)}{11.93}\right]^{17.79}. \tag{54}$$

We first compute $L_{\mathrm{AGN}}^{\mathrm{bol}}(\tau) = \int_0^\infty \mathrm{d}\lambda\, L_{\mathrm{AGN}}(\lambda, \tau) = f_{\mathrm{AGN}} L_{\mathrm{dust}}(\tau)/(1 - f_{\mathrm{AGN}})$ from Eq. (53) and then use Eq. (54) to obtain the spectrum normalisation $L_{\mathrm{AGN}}^{X}(\tau)$ in the hard X-ray band 2–10 keV.

F06 templates are excellent for modelling AGNs for which the geometry is well known and/or when the AGN contribution is dominant over the spectrum. Nonetheless, due to their high number of dimensions, they prove to add a level of complexity to the model that would require extremely large datasets to produce

significant parameters posteriors if used for fitting. Furthermore, our current implementation of the X-Ray emission from AGN does not account for the torus attenuation nor for that due to galactic dust and, therefore, should also be included carefully. The purpose of the current implementation of the AGN module in GalaPy is to add a already known AGN emission to the overall spectrum, when needed. We plan to extend GalaPy with a self-consistent parameterised modelling of the AGN accounting for BH-galaxy co-evolution and clumpy torus emission in the nearest future. This extension will be intended for continuous exploration of the parameter space within the Bayesian framework of the library.

## 2.6. Build a galaxy model

The overall rest-frame SED is obtained by summing all the contributions from the components building up the galaxy model of choice. The default minimal set-up provides a total emission given by

$$L_{\mathrm{TOT}}^{\mathrm{default}}(\lambda, \tau) = L_{\mathrm{CSP}}^{\mathrm{a}}(\lambda, \tau) + L_{\mathrm{MC}}(\lambda, \tau) + L_{\mathrm{DD+PAH}}(\lambda, \tau), \tag{55}$$

where the different terms are computed via the relevant equations provided in the previous sections. Including all the optional components to the galaxy model will produce an SED given by

$$L_{\mathrm{TOT}}(\lambda, \tau) = L_{\mathrm{TOT}}^{\mathrm{defaul}}(\lambda, \tau) + L_{\mathrm{NFF}}(\lambda, \tau) + L_{\mathrm{syn}}^{\mathrm{corr}}(\lambda, \tau) +$$
$$L_{\mathrm{AGN}}(\lambda, \tau) + L_{\mathrm{XRB}}(\lambda, \tau). \tag{56}$$

We provide a convenient class GXY that can be instantiated by importing it from the galapy.Galaxy module. This class manages the interplay between all the components and provides access to all the free-parameters tuning. It can both be used for building mock SED observations and for modelling emission. A summary of all the tunable parameters available through this interface is reported in Appendix B.2 and in Table B.3.

### 2.6.1. Cosmology and redshifting

When dealing with the emission from galaxies, choosing a cosmological model plays a primary role in deriving the flux received by an observer at a given distance from the source, along with a secondary role in imposing an upper limit to the age the modelled galaxy can have. Given these considerations, we implemented a Cosmology class with limited functionalities but significant flexibility. It is built by passing two grids used for interpolation: a redshift-luminosity distance grid and a redshift-cosmic age grid. Along with the possibility to provide directly grids computed with external libraries (such as with e.g. astropy, The Astropy Collaboration 2013), we provide several ready-to-use popular parameterisations in our database that can be chosen easily by passing the relevant string (e.g. 'Planck2018' for rounded Planck Collaboration VI 2020 parameters[6]).

For a galaxy at redshift $z$, we compute the observed SED in terms of flux density $S_\nu(\lambda_{\mathrm{O}})$ in mJy at the observation wavelength $\lambda_{\mathrm{O}} = \lambda_{\mathrm{R}}(1 + z)$ by redshifting the rest-frame SED,

---

[6] This choice is driven by the requirement to limit the number of external dependencies of GalaPy. See the online documentation for a complete list of available cosmological models and for instructions on how to use custom additional models not present in the database.
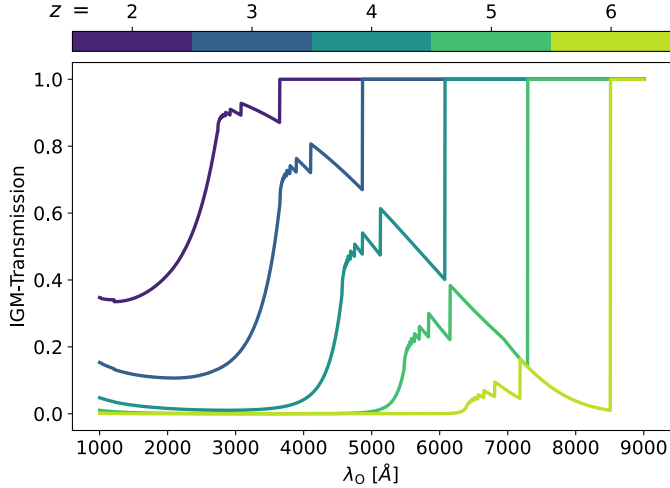
**Fig. 13.** Overall IGM transmission functions predicted by Inoue et al. (2014) for different values of redshift (colour-coded).

converting it from energy to flux via the cosmological luminosity distance $D_L(z)$

$$S_\nu(\lambda_O) \equiv \frac{\lambda_R^2 L_{TOT}(\lambda_R, \tau)}{4\pi D_L^2(z)} \times \frac{(1+z)}{c} \tag{57}$$

expressed as a function of the rest frame wavelength, $\lambda_R$ and where $L_{TOT}(\lambda_R, \tau)$ is given by Eq. (56).

### 2.6.2. Intergalactic medium

The main contribution to the damping of ultra-violet photons due to the absorption from the intergalactic medium (IGM) is ascribed to hydrogen, with a minor contribution from heavier elements. To model this effect we exploit the fitting functions from Inoue et al. (2014), provided in terms of piece-wise equations for the Lyman-series (LS) and Lyman-continuum (LC) absorption from Damped Lyman-$\alpha$ systems (DLA) and from the Lyman-$\alpha$ Forest (LAF). The authors approximated model provides a fair trade-off between accuracy and performance.

The optical depth is then given by the sum of the various contributions:

$$\tau_{IGM}(\lambda_O, z) = \tau_{LC}^{LAF}(\lambda_O, z) + \tau_{LS}^{LAF}(\lambda_O, z) + \tau_{LC}^{DLA}(\lambda_O, z) + \tau_{LS}^{DLA}(\lambda_O, z) \tag{58}$$

where the different terms are computed from Eqs. (20), (21) and (25)–(29) of Inoue et al. (2014).

As a result, the observed flux of Eq. (57) is multiplied by a transmission term given by $e^{-\tau_{IGM}(\lambda_O, z)}$. In Fig. 13, we show this transmission for different values of redshift above $z = 2$.

### 2.6.3. Photometry and spectroscopy

GalaPy is capable of generating synthetic spectra from extra-galactic sources at the native resolution of the input SSP library used. To compute fluxes in the observational band-pass filters, we use the transmission function $T_i(\lambda)$ in units of photons[7]

---

[7] In case of energy counter detectors we make the replacement

$$T(\lambda) \rightarrow T(\lambda)/\lambda.$$

associated with each instrumental filter, $i$. We obtain the band-averaged flux as:

$$\overline{S}_i = \frac{\int_0^\infty d\lambda\, T_i(\lambda)\, S(\lambda)/\lambda}{\int_0^\infty d\lambda\, T_i(\lambda)/\lambda}, \tag{59}$$

where the flux $S(\lambda)$ is computed through Eq. (57). Band emission can be associated with a typical, 'pivot' wavelength of the filter:

$$\overline{\lambda}_i \equiv \sqrt{\frac{\int_0^\infty d\lambda\, \lambda T_i(\lambda)}{\int_0^\infty d\lambda\, T_i(\lambda)/\lambda}}. \tag{60}$$

In our database, a set of band-pass transmissions from popular experiments is made available (e.g. JWST, SDSS, HST, *Spitzer*, *Herschel*, ALMA, VLA), but users can also load their custom transmissions by providing a wavelength-transmission grid over which the system should interpolate the function $T(\lambda)$.

A utility class `PhotoGXY` can be instantiated by importing the `galapy.Galaxy` module. Objects of `PhotoGXY` type allow the user to provide a photometric system to simulate and model observations on a set of band-pass transmissions of choice.

At current stage of development, the library does allow for fitting both photometric and spectroscopic datasets. Nonetheless, this requires us to modify the default likelihood from the python API (tutorials are available in the documentation). Automatised sampling of the parameter space with spectroscopic datasets will be the subject of a focussed forthcoming work in the GalaPy series.

## 3. Parameters inference and analysis

In GalaPy, we use Monte Carlo techniques in a Bayesian framework in order to sample the posterior probability distributions in the parameter space defining our galaxy models. A `sampling` sub-module is accessible from the Python API which provides an interface to two popular pure-Python libraries for parameter-space sampling, `emcee` (Foreman-Mackey et al. 2013) and `dynesty` (Speagle 2020). The two libraries offered by GalaPy provide distinct techniques and philosophies for addressing the challenge of multi-dimensional sampling.

We describe here our current implementation and default set-up of the hyper-parameters[8], highlighting though that the sampling module of GalaPy will be extended in future developments of the library. For the latest functionalities of the library, users should always refer to the on-line documentation. Furthermore, all the discussion below only refers to the out-of-the-box functionalities, accessed through the entry-points described in Appendix C, that can always be extensively customised by accessing the GalaPy Python API.

### 3.1. Statistical set-up: Likelihood, noise, and priors

In GalaPy, parameter space is sampled with the intent of maximising the log-likelihood

$$\ln \mathcal{L}\left(\overline{S}\,|\,\theta\right) \equiv -\frac{1}{2}\chi^2\left(\overline{S}\,|\,\theta\right) \tag{61}$$

---

[8] This hyper-parameters, including prior sizes, free model parameters and sampling strategy, can be set through the parameter-file generated calling the `galapy-genparams` command.